nature astronomy

Article

https://doi.org/10.1038/s41550-025-02749-7

A detection of sulfur-bearing cyclic hydrocarbons in space

Received: 30 May 2025

Accepted: 21 November 2025

Published online: 23 January 2026

Check for updates

Mitsunori Araki [1] ✉, Miguel Sanz-Novo [2], Christian P. Endres [1], Paola Caselli [1], Víctor M. Rivilla [2], Izaskun Jiménez-Serra [2], Laura Colzi [2], Shaoshan Zeng [3], Andrés Megías [2], Álvaro López-Gallifa [2], Antonio Martínez-Henares [2], David San Andrés [2,4], Sergio Martín [5,6], Miguel A. Requena-Torres [7], Juan García de la Concepción [8] & Valerio Lattanzi [1] ✉

Molecules harbouring sulfur are thought to have played a key role in the biological processes of life on Earth, and thus, they are of much interest when found in space. Here we report on the astronomical detection of a six-membered sulfur-bearing cyclic hydrocarbon in the interstellar medium. Observations of the Galactic Centre molecular cloud G+0.693-0.027 reveal the presence of 2,5-cyclohexadien-1-thione, which is a structural isomer of thiophenol (*c*-C_6H_6S). For the astronomical identification, we first performed precise laboratory measurements of the thiophenol discharge products system. These measurements, conducted in the radio band using a chirped-pulse Fourier transform microwave spectrometer, enabled us to characterize this highly polar molecular species and provided unambiguous fingerprints needed to identify this organosulfur compound in space, which now ranks as the largest interstellar sulfur-bearing molecule. These results herald the discovery of a family of prebiotically relevant sulfur-bearing species, which potentially act as a bridge between the chemical inventory of the interstellar medium and the composition of the minor bodies of the Solar System.

Understanding the origin of life remains one of the most profound and enduring challenges in science. Over many years, numerous theories have been advanced to address this question (for example, ref. 1). Among these, the hypothesis that life's building blocks were synthesized in interstellar space and later delivered to the primitive Earth via comets and meteorites has garnered substantial attention[2,3]. This model is supported by the detection of a rich inventory of prebiotic organic molecules in comets (for example, refs. 4,5), meteorites (for example, ref. 6) and asteroids (for example, refs. 7,8).

The role of sulfur-bearing molecules is pivotal in the general discussion of prebiotic chemistry. Sulfur (S) is indispensable to many biological processes and is considered an essential element for life on Earth (for example, ref. 9). Yet, there exists a notable discrepancy between the S compounds observed in interstellar space and those found in meteoritic material. In the gas phase of the interstellar medium (ISM), only a limited array of S species—predominantly small molecules with up to nine atoms (CH_3SCH_3 (ref. 10) and C_2H_5SH (refs. 11,12))—have been detected. Furthermore, whereas the observed sulfur abundance in the

[1]Center for Astrochemical Studies, Max-Planck-Institut für extraterrestrische Physik, Garching, Germany. [2]Centro de Astrobiología (CAB), CSIC-INTA, Torrejón de Ardoz, Spain. [3]Star and Planet Formation Laboratory, Cluster for Pioneering Research, RIKEN, Wako, Japan. [4]Departamento de Física de la Tierra y Astrofísica, Facultad de Ciencias Físicas, Universidad Complutense de Madrid, Madrid, Spain. [5]European Southern Observatory, Vitacura, Chile. [6]Joint ALMA Observatory, Vitacura, Chile. [7]Department of Physics, Astronomy and Geosciences, Towson University, Towson, MD, USA. [8]Departamento de Química Orgánica e Inorgánica, Facultad de Ciencias, and IACYS-Green Chemistry and Sustainable Development Unit, Universidad de Extremadura, Badajoz, Spain. ✉e-mail: araki@mpe.mpg.de; lattanzi@mpe.mpg.de

diffuse ISM is consistent with the cosmic value, the overall abundance of gas-phase S species in dense molecular clouds is significantly lower (for example, one order of magnitude lower[13]) than expected compared with the cosmic S/H abundance ratios. This S depletion in the ISM indicates that a substantial fraction of sulfur may be sequestered in forms that are not readily detectable, such as refractory compounds or as constituents of dust grains, leaving the dominant carriers of sulfur in interstellar space unidentified.

By contrast, meteoritic analyses have consistently uncovered a diverse suite of larger S-bearing molecules, most of which contain more than nine atoms, for example, benzothiophene C_8H_6S (refs. 6,14,15). The absence of these larger, potentially prebiotically relevant S species in the ISM raises critical questions about the chemical evolution that bridges interstellar matter and the chemical composition of cometesimals and planetesimals. It is possible that our current observational capabilities are insufficient to detect these elusive large compounds in the ISM or that substantial chemical transformations occur during the transfer from interstellar clouds to planetary surfaces, such as the early Earth.

To date, more than 340 interstellar molecules have been detected in the ISM and circumstellar envelopes[16,17]. The record of these discoveries is characterized not merely by a gradual increase in numbers but also by the episodic emergence of entirely new molecular groups. The most recent breakthrough occurred following the detection of benzonitrile by McGuire et al.[18] in 2018 within Taurus Molecular Cloud 1. Subsequently, several cyclic hydrocarbon cyanides have been identified, with 1- and 2-cyanonaphthalene (c-$C_{10}H_7CN$) being recognized as the first polycyclic hydrocarbons[19]. Following this, tetracyclic hydrocarbon cyanides, such as 1-, 2- and 4-cyanopyrene (c-$C_{16}H_9CN$)[20,21] were found in 2024. At present, the largest interstellar molecule, apart from fullerenes, is the seven-ring polycyclic aromatic hydrocarbon (PAH) cyanocoronene (c-$C_{24}H_{11}CN$)[22]. It is important to note that the cyclic hydrocarbons detected include not only cyanide species but also pure hydrocarbons, for example, ethynylbenzene (c-C_6H_5CCH)[23]. Among these, indene (c-C_9H_8), a bicyclic hydrocarbon, is the largest species identified to date[24]. In total, 17 cyclic hydrocarbon species, including benzene[25], have been observed. In a natural progression of these findings, Yang et al.[26] proposed that S-bearing PAHs, particularly those incorporating S heterocycles, might serve as a reservoir for the missing S. This proposal is supported by the detection of compounds such as thiophenol (c-C_6H_5SH)[6], diphenyl disulfide, dibenzothiophene, thianthrene[14] and thiophene along with related species[15] in meteorites. Nevertheless, although S-bearing species account for approximately 15% of the interstellar molecules detected, S-bearing cyclic hydrocarbons have yet to be identified in interstellar space except for the claimed detection of the small species c-C_3H_2S (ref. 27), possibly due to their missing spectral experimental characterization.

Thiophenol is one of the most fundamental of the S-bearing cyclic hydrocarbons and has been detected in meteoritic material. However, its dipole moment is relatively small (a- and b-dipole moments: μ_a = 0.83 D and μ_b= 0.75 D; Extended Data Table 1), which might be a main limiting factor for its possible identification in the interstellar gas through millimetre-wave astronomical observations. Also, the rotation of the SH group relative to the phenyl ring causes a splitting of its rotational lines and, hence, an overall spread of its emitted intensity (and, therefore, molecular population) across a higher number of rotational levels. By contrast, 2,5- and 2,4-cyclohexadien-1-thione (two isomeric forms of c-C_6H_6S, hereafter 2,5-CT and 2,4-CT, respectively; a-type dipole moments: 4.73 D and 3.87 D; Extended Data Table 1), which are structural isomers of thiophenol, do not exhibit splitting due to spin–rotation interactions, internal rotation or hyperfine effects. These rigid molecules display a pure rotational spectrum characteristic of an asymmetric top—analogous to the behaviour observed by 2,5- and 2,4-cyclohexadien-1-one (c-C_6H_6O)[28]—and, as discussed later, they have substantially larger dipole moments. Consequently, the rotational lines of these two species might be brighter than those of their most stable isomeric form, rendering them favourable for interstellar detection in molecular clouds. Similar cyclic hydrocarbons incorporating a doubly hydrogenated carbon (–CH_2–) within their ring structures, have already been detected in interstellar gas (for example, cyclopentadiene[29], ethynyl cyclopentadiene[29], indene[24], 1-cyanocyclopentadiene[30] and 2-cyanocyclopentadiene[31]), stressing the potential interest of these thiophenol isomers for interstellar detection.

We report here the discovery of 2,5-CT, the largest S-bearing molecule detected so far, towards the Galactic Centre molecular cloud G+0.693-0.027 (hereafter, G+0.693). Situated within the Sgr B2 complex, this source is one of the principal reservoirs of complex organic molecules (having six or more atoms in total) in our Galaxy and has been the site of over 20 first interstellar detections (see, for example, refs. 32–35). We selected G+0.693 for our search for 2,5-CT due to its exceptional richness in S-bearing species[10,12,36–38] and because the aromatic ring benzonitrile has also been recently detected (Rivilla, V. M., private communication). This chemical diversity is probably attributable to the enhanced sputtering of icy grain mantles induced by large-scale shocks from cloud–cloud collisions, which release a significant fraction of the S budget expected to be locked in interstellar ices[39].

Results and discussion

Laboratory identification

The experimental search for 2,5-CT and 2,4-CT was guided by ab initio quantum chemical calculations that derived the main spectroscopic parameters from geometry optimization and harmonic force field analysis (section 'Theoretical calculations' and Extended Data Fig. 1). The rotational transitions of 2,5-CT and 2,4-CT in the 8–40-GHz range were observed using a combination of a chirped-pulse Fourier transform microwave spectrometer and a pulsed-discharge supersonic jet (section 'Laboratory measurements' and Extended Data Figs. 2 and 3 for details). Molecules were generated by a pulsed discharge in the throat of a 10-Hz supersonic jet using a vapour pressure of thiophenol at room temperature of 25 °C. The experimental settings were optimized by monitoring the production of 2,5- and 2,4-cyclohexadien-1-one generated from the discharge of anisole (c-$C_6H_5OCH_3$).

In the 8–40-GHz region, 92 and 75 rotational lines of 2,5-CT and 2,4-CT, respectively, were detected, covering quantum numbers up to J = 15 and K_a = 7, as shown in Supplementary Data 1 and 2 (ref. 40). Their rest frequencies, determined with a precision of about 5 kHz, were fitted to an effective Watson-type Hamiltonian in S reduction, which included the rotational and centrifugal distortion constants listed in Table 1. The three rotational constants A_0, B_0 and C_0 and the centrifugal distortion constants D_J, D_{JK}, d_1 and d_2 were determined by the fit, whereas the centrifugal distortion constant D_K was kept fixed to the values obtained by the CAM-B3LYP/cc-pCVTZ calculations[41,42]. The fit reproduces the experimental frequencies with a root-mean-square (RMS) deviation of 2.8 kHz and 3.3 kHz for 2,5-CT and 2,4-CT, respectively. Based on this analysis, rest frequencies for transitions used in the analysis of the astronomical spectra are predicted with uncertainties sufficiently better than 10 kHz. For the frequency ranges of the spectroscopic survey carried out towards the G+0.693 cloud, this uncertainty corresponds to uncertainties in velocity of less than 0.1 km s^{-1}. This is small compared with the typical linewidths of the molecular emission measured towards this cloud (of ~20 km s^{-1}; ref. 39).

Detection of 2,5-CT in G+0.693

We analysed an unbiased, ultrasensitive broadband spectral survey of G+0.693 carried out with the IRAM 30-m and Yebes 40-m radio telescopes (for details of the observations, see Methods). The observed data were compared with simulated spectra of 2,5-CT generated with the Spectral Line Identification and Modeling (SLIM) tool within the MADCUBA software package[43], under the assumption of constant excitation temperature, here referred to as local thermodynamic

Table 1 | Molecular parameters for 2,5-CT and 2,4-CT derived from the least square fits

Parameter		2,5-CT		2,4-CT	
		Observed	Calculated	Observed	Calculated
A_0	MHz	5,285.4602(38)	5,309.7	5,216.7958(46)	5,271.8
B_0	MHz	1,608.45219(13)	1,618.3	1,619.66382(15)	1,623.9
C_0	MHz	1,242.73075(11)	1,249.7	1,247.58786(13)	1,253.1
D_J	kHz	0.05122(19)	0.049	0.06686(24)	0.054
D_{JK}	kHz	0.2562(24)	0.260	0.1806(70)	0.272
D_K	kHz	0.977377	0.977377	0.908029	0.908029
d_1	kHz	−0.01438(19)	−0.014	−0.01527(22)	−0.015
d_2	kHz	−0.00281(14)	−0.003	−0.00240(20)	−0.0022
Number of lines		92		75	
RMS	kHz	2.8		3.3	

The spectroscopic constants in the S-reduced Hamiltonian in the I′ representation were fitted using the program SPFIT[60], and the uncertainties of the spectroscopic parameters obtained were evaluated by the program PIFORM[40]. Standard uncertainties are given in parentheses. Parameters without uncertainties were kept fixed to the values obtained by the quantum chemical calculation. The calculated rotational constants were derived from the equilibrium values (B_e) at the cc-pCV5Z level with the vibrational corrections (B_e−B_0) estimated using cc-pCVTZ. Centrifugal distortion constants were calculated at cc-pCVTZ. RMS stands for root-mean-square error.

equilibrium (LTE). We note that the intermediate H_2 volume densities (10^4–10^5 cm^{-3}) in G+0.693 (refs. 39,44) result in the subthermal excitation of molecular emission, thus yielding excitation temperatures (T_{ex} = 5–20 K, which is lower than the kinetic temperature T_k = 50–150 K; ref. 39). Unlike massive hot cores or low-mass hot corinos—where numerous rotational transitions, including those from vibrationally excited states, are observed—only low-energy rotational transitions in the ground vibrational state are detectable in G+0.693, significantly reducing the levels of line blending and confusion due to the excitation temperatures. Consequently, with the current sensitivity, we anticipate the detection of a few tens of transitions of 2,5-CT at these low excitation temperatures.

After assessing the emission of more than 140 molecules previously identified towards G+0.693, we detected many a-type transitions of 2,5-CT with an integrated signal-to-noise ratio >5 covering from the upper rotational levels J_{up} = 12 to 19, including several pairs of transitions belonging to two nearly complete progressions of $(J+1)_{0,J+1} \leftarrow J_{0,J}$ and $(J+1)_{1,J+1} \leftarrow J_{1,J}$ transitions (Fig. 1a), with the exception of the $12_{1,12}$–$11_{1,11}$ transition, which lies out of the covered frequency range, and the $17_{1,17}$–$16_{1,16}$ and $17_{0,17}$–$16_{0,16}$ transitions, which seem to be heavily blended with unidentified lines. These pairs of lines progressively converge as the frequency increases, eventually coalescing into a doubly degenerate line for J_{up} = 19. Overall, we found 22 unblended or slightly blended features, the latter being contaminated by less than 25% (Fig. 1; spectroscopic information is listed in Extended Data Table 2, including an analysis of the contamination). These were subsequently used in the LTE fitting and to derive the physical parameters of 2,5-CT (detailed information about the LTE fitting using the MADCUBA-SLIM tool and the definition of an unblended line is provided in the Methods section). We stress that no missing lines were observed within the whole dataset, and the remaining lines were either heavily blended or too weak to be observed (transitions at 2 mm and 3 mm that did not rise above the noise). Our results are in agreement with the observed spectra.

The best-fitting LTE model for 2,5-CT (shown in red in Fig. 1) yields an excitation temperature T_{ex} = 14.3 ± 3.4 K, a radial velocity v_{LSR} = 71.7 ± 0.9 km s^{-1}, a linewidth with a full-width at half-maximum (FWHM) of 20.0 km s^{-1} and a molecular column density $N = (5.6 \pm 0.3) \times 10^{12}$ cm^{-2}, which translates into a fractional abundance with respect to H_2 of $(4.1 \pm 0.7) \times 10^{-11}$, using $N(H_2) = 1.35 \times 10^{23}$ cm^{-2} as derived by ref. 45. A complementary population diagram analysis has also been performed[46], which gave physical parameters that are in good agreement with the SLIM-AUTOFIT analysis: $N = (5.6 \pm 1.4) \times 10^{12}$ cm^{-2} and T_{ex} = 12.5 ± 1.5 K (Methods section and Extended Data Fig. 4). The partition functions used are listed in Extended Data Table 3.

Astrophysical implications

The detection of 2,5-CT opens a new window into the chemistry of large S-bearing cyclic molecules in the ISM, and it provides the first basis for elucidating their abundance and formation. The most straightforward comparison is between 2,5-CT and its structural isomers, 2,4-CT and thiophenol, which are not clearly detected in the current astronomical data (Methods section). Based on the derived upper limits for both molecules (N(2,4-CT) ≤ 3.2×10^{12} cm^{-2} and N(thiophenol) ≤ 8×10^{13} cm^{-2}), we expect that 2,5-CT is more than twice as abundant as 2,4-CT (which is close to the factor of ~2 estimated in our laboratory from the relative intensities of rotational lines) whereas N(thiophenol)/N(2,5-CT) < 14. Of the two structural isomers, 2,4-CT and 2,5-CT, it would be expected from the energy level diagram (Extended Data Fig. 1) that the low-energy one would be more abundant, in agreement with the detection, but the relatively low dipole moment of thiophenol compared with those of both 2,5-CT and 2,4-CT (Extended Data Table 1) prevents us from unveiling conclusively whether only 2,5-CT is selectively produced in the ISM or whether 2,4-CT and thiophenol are also present but remain undetected due to sensitivity limitations. Besides the emergence of 2,5-CT as the only structural isomer identified to date for the C_6H_6S family, our findings now confirm the existence of large (more than ten atoms) sulfur-containing cyclic species in the ISM. Although 2,5-CT itself accounts for only a small fraction of the S budget detected towards G+0.693 so far (~0.05%; Sanz-Novo, private communication), its discovery may be just the tip of the iceberg of a yet unexplored chemistry. This scenario might closely mirror that of benzonitrile, whose initial detection in the ISM by McGuire et al.[18] preceded the discovery of numerous cyano-substituted PAHs, and is in line with the rich inventory of S-bearing rings in meteorites, with over 80 species detected (including thiophenol, dibenzothiophene and thianthrene[6,14]. By analogy with the nearly flat abundance trend of cyano-bearing rings found in Taurus Molecular Cloud 1[20,22], the cumulative contribution of the C_6H_6S isomers in G+0.693 could approach ~1.5% of the total S reservoir, hinting that S-bearing cyclic hydrocarbons and S-bearing PAHs might not represent a relevant sink of sulfur in the ISM. In this context, if a small portion of sulfur is locked up in S-bearing PAHs and related S-containing cyclic species, we anticipate that the James Webb Space Telescope is capable of detecting several infrared features[26], even though some of the prominent bands (for example, the 10-μm C–S-band) may be obscured by the 9.7-μm silicate absorption band.

https://doi.org/10.1038/s41550-025-02749-7

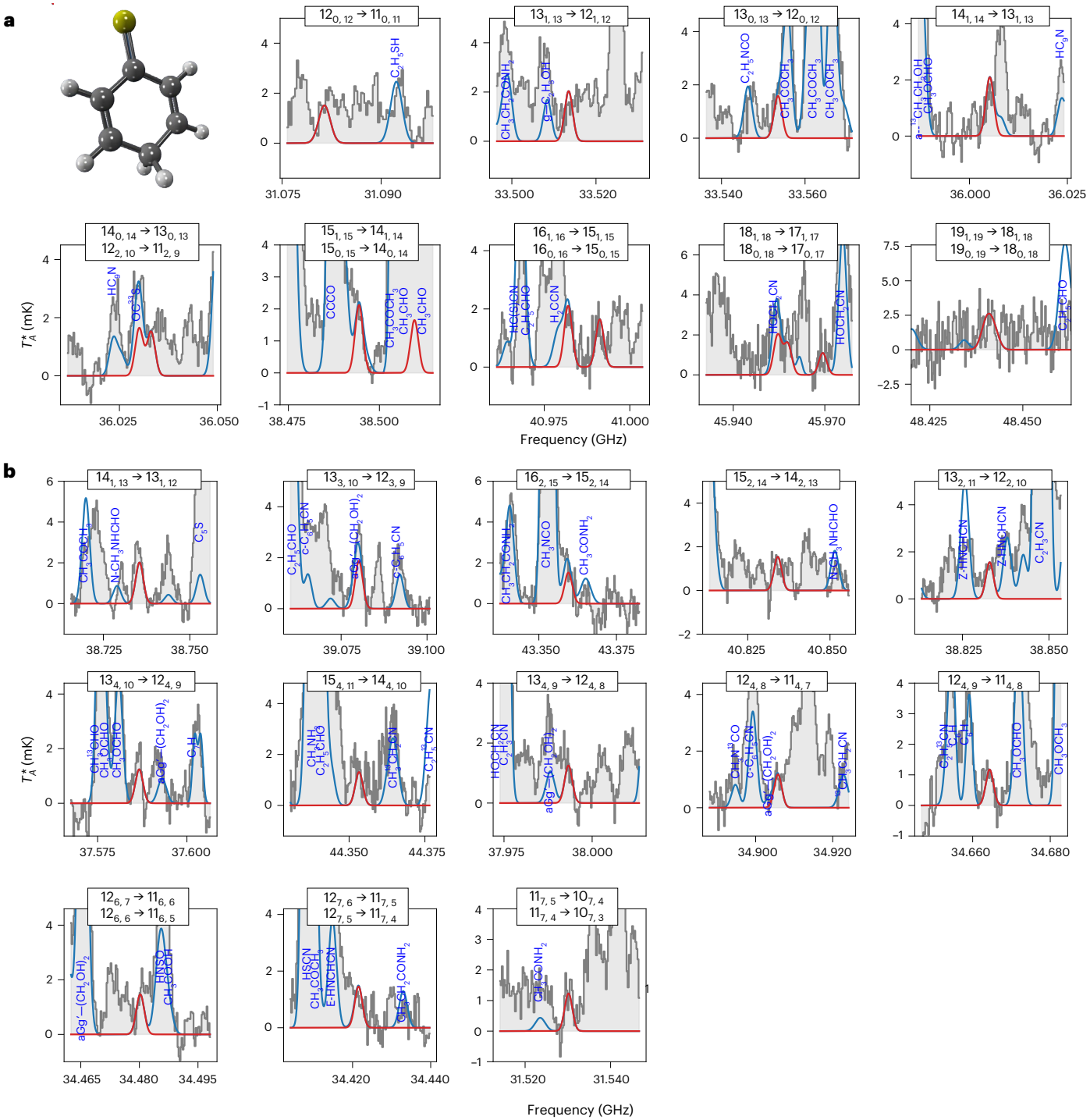

Fig. 1 | Lines of 2,5-CT detected towards the Galactic Centre molecular cloud G+0.693. a, Pairs of $K_a = 0$ and 1 transitions that progressively converge with increasing frequency, ultimately coalescing into a doubly degenerate line. **b**, $K_a > 1$ transitions of 2,5-CT observed in the astronomical data that were also used to derive the LTE physical parameters of the molecule (see text; listed in Extended Data Table 2). The quantum numbers for each transition are shown in the upper part of each panel. The red lines depict the result of the best LTE fit to the 2,5-CT rotational transitions. The blue lines are the emission from all the molecules identified to date in the survey, including 2,5-CT, overlaid with the observed spectra (grey histograms and light grey shaded area). The three-dimensional structure of 2,5-CT is also shown (carbon atoms in grey, S atom in yellow and hydrogen atoms in white).

Moreover, upcoming radioastronomical facilities, such as the Square Kilometre Array or the Atacama Large-Aperture Submillimeter/millimeter Telescope, will probably find a rich reservoir of large cyclic S-bearing species, including potentially prebiotic molecules.

The detection of 2,5-CT can be rationalized in terms of its large dipole moment (a-type dipole moment $\mu_a = 4.73$ D; Extended Data Table 1). This result establishes this organosulfur species as a promising observational link between the rich S inventory found in the minor bodies of the Solar System (asteroids, comets and meteorites), which includes a wide array of cyclic S-bearing compounds, ranging from thiophenol[6] and thiophene[15] to the more complex diphenyl disulfide, dibenzothiophene and thianthrene[14], and the known S budget in the ISM, which has been limited so far to the detection of molecules with up to nine atoms[10–12]. With 13 atoms, 2,5-CT now ranks as the largest

S-bearing molecule detected so far in the ISM, marking an important step forwards in molecular size and complexity within interstellar sulfur chemistry. Previously, the largest S-bearing interstellar species had up to nine atoms (for example, ethyl mercaptan, CH_3CH_2SH, and its isomer dimethyl sulfide, CH_3SCH_3 (refs. 10,12)). In this context, 2,5-CT is the largest S-bearing complex organic molecule detected so far and also the most complex S-bearing cyclic species. Thus, it provides a novel view on cyclic interstellar chemistry, which now extends beyond pure hydrocarbons and their cyano (–CN) and ethynyl (–CCH) derivatives. Additionally, our findings highlight the need for caution when analysing mass spectrometric measurements of cometary, meteoritic and asteroid material targeting thiophenol, as the mass peak could be contaminated by 2,5-CT, given that both molecules share the same molecular mass (110.02 u). Consequently, although 2,5-CT has not, to our knowledge, been searched for in extraterrestrial material from these minor bodies, it may still be present but unidentified.

To date, the potential formation routes for 2,5-CT and related S rings remain largely unexplored, both experimentally and theoretically. Consequently, we can only hypothesize its possible formation routes by either studying chemically related species or by drawing analogies with bottom-up pathways proposed for related cyclic species. Given the uncertain efficiency of gas-phase pathways, such as those invoked for benzene formation through ion–molecule reactions[47], which are considered to be the bottleneck in the growth of larger PAHs, a potential dust-grain origin appears particularly promising in G+0.693. Laboratory simulations have shown that cosmic-ray irradiation of low-temperature acetylene (C_2H_2) ices efficiently produces benzene[48], indicating that an analogous chemistry involving small S-bearing carbon chains (for example, C_2S and C_3S, and also the detection in the ISM of up to the five-carbon member, C_5S; ref. 49) and C_2H_2 on icy grains could lead to 2,5-CT. Although this hypothesis still needs to be tested in the laboratory, it is supported by two key factors that shape the chemistry of G+0.693, where linear S chains are also abundant (for example, $N(CCS) = 1.5 \times 10^{14}$ cm^{-2}): (1) Its elevated cosmic-ray ionization rate (10^{-14}–10^{-15} s^{-1}), estimated through chemical modelling involving cations such as PO^+ and $HOCS^+$ (ref. 37 and references therein), which favours radical formation and recombination on grain mantles[34]. (2) The occurrence of large-scale low-velocity shocks associated with a cloud–cloud collision scenario[50], which enhance the sputtering of icy grain mantles and could facilitate the desorption of molecules such as 2,5-CT. An analogous connection has already been suggested between benzonitrile, which is also detected in G+0.693 (Rivilla, V. M., private communication), and the cyanopolyyne family[51], but for 2,5-CT, the inclusion of ring defects (a $(-CH_2-)$ moiety that disrupts the electron delocalization and, thus, the aromaticity within the ring) needs to be addressed. Alternatively, benzene could be directly released from the grains through shocks and subsequently react through radical–neutral reactions[52,53], which are considered to be some of the main formation routes for diverse PAHs, such as *c*-C_6H_5CN (ref. 18), *c*-$C_{10}H_7CN$ (ref. 19), *c*-C_5H_5CN (ref. 30) and *c*-$C_{16}H_9CN$ (refs. 20,21). However, apart from a recent study on the production of *c*-C_3H_2S via *c*-C_3H_2 + SH (ref. 27), there are no theoretical or experimental data that support an analogous formation route starting from *c*-C_6H_6 and yielding 2,5-CT or any of its isomers (for example, thiophenol).

In summary, the study of interstellar chemistry of large cyclic species (>12 atoms) has been bound so far to pure cyclic hydrocarbons or cyano (–CN) and ethynyl (–CCH) derivatives, as their derivatization provides a sizeable dipole moment to the parental, typically nonpolar hydrocarbon (for example, benzene, naphthalene or pyrene), thus enabling their radioastronomical identification. The interstellar detection of 2,5-CT presented here, which is based on new high-resolution rotational data, demonstrates that interstellar cyclic chemistry extends beyond the aforementioned families to encompass S-bearing compounds. These findings open the window to a yet uncharted S chemistry, which, although it might not account for the missing sulfur in dense interstellar environments, does contribute considerably to our understanding of the origin of sulfur-containing molecules in meteorites and comets and provides insight into sulfur reservoirs in young solar-type systems.

Methods

Theoretical calculations

All the quantum chemical calculations were carried out with ORCA[54] using CAM-B3LYP[41]. The correlation-consistent polarized core-valence quintuple-zeta basis set (cc-pCV5Z)[42] was used for molecular geometry optimizations and energy calculations of thiophenol, 2,5-CT and 2,4-CT. Effective rotational constants and centrifugal distortion constants for 2,5-CT and 2,4-CT were evaluated theoretically at cc-pCVTZ through harmonic force field calculations. The calculated energies and dipole moments are listed in Extended Data Table 1; the rotational and centrifugal distortion constants are shown in Table 1 along with their experimental values. The accuracy of the dipole moments is expected to be around 8.5% based on comparisons of the values calculated by this method with the observed dipole moments for H_2S, dimethylsulfide, thiophene and 3-methylthiophene.

Laboratory measurements

High-resolution rotational spectra of 2,5-CT and 2,4-CT were observed using a high-resolution broadband microwave spectrometer in combination with a pulsed-discharge supersonic jet, as shown in Extended Data Figs. 2 and 3.

Pulsed-discharge supersonic jet. Molecules of 2,5-CT and 2,4-CT were generated via pulsed discharge in a 10-Hz supersonic jet (CASJet[55]) using thiophenol (Thermo Fisher Scientific, without further purification) maintained at its vapour pressure at room temperature (25 °C) and diluted in neon as a buffer gas with a flow of 50–55 sccm. The jet was produced with a pulse valve (Parker) controlled by a pulse driver (IOTA ONE, Parker). By employing a backing pressure of ~1 kTorr, the molecular beam was cooled to a rotational temperature of approximately 5 K, as estimated from the relative line intensities of thiophenol. Under these conditions, the pressure in the vacuum chamber was maintained at approximately 0.5×10^{-4} Torr to 1.0×10^{-4} Torr using a combination of a diffusion pump, a root blower and a rotary pump.

The discharge nozzle, mounted directly after the pulse valve, comprised electrodes made of small copper discs with a thickness of 3 mm, each featuring a central aperture through which the molecular beam flowed—4.3 mm for the downstream electrode and 2.3 mm for the upstream electrode. The downstream electrode was grounded and served as the anode, whereas the upstream electrode was negatively charged and functioned as the cathode. These electrodes were separated by a Teflon insulator cylinder (13.4 mm in length with a 3.5 mm central aperture) and connected in series with a 50-kΩ ballast resistor. A voltage of 1,000 V was applied across the assembly, resulting in a current of a few milliamperes. Under these conditions, a plasma discharge was generated between the electrodes immediately before the supersonic expansion in the vacuum chamber.

The chirped-pulse Fourier transform microwave spectrometer. The chirped-pulse Fourier transform spectrometer is a high-resolution broadband instrument covering frequencies in the range 8–40 GHz. An intense pulse of length 2 μs, chirped in frequency, produced a macroscopic polarization of the molecular sample. The subsequent free induction decay was recorded in the time domain using a heterodyne receiver. A two-channel arbitrary waveform generator (Keysight, M8190A) generated the chirped pulse, which was frequency upconverted using an IQ modulator and a tunable signal generator (Agilent Technologies, E8257D) to cover the frequencies of interest (8–18 GHz, 18–26 GHz and 26–40 GHz). A solid state amplifier (8–18 GHz: Microsemi C0618-43-T680; 18–26 GHz: Microsemi C1826-36-T964 and 26–40 GHz: Eravant SBP-2734033530-KFKF-S1-HR) amplified the signal before it was emitted via a quad ridge horn antenna, the other port

of which was used to detect the molecular signal. A rooftop mirror in the chamber was used to rotate the polarization by 90°. The receiver consisted of a low-noise amplifier protected from the intense excitation pulse by a fast pin diode switch, followed by an identical IQ modulator using the same local oscillator signal to downconvert the free induction decay. The intermediate frequency (IF) signal was then fed into a 5-GHz low pass filter, which was followed by another amplifier, before being digitized using an Acqiris U9510A digitizer card. The measurements were repeated and averaged in the time domain to improve the signal-to-noise ratio. During the measurements, the phase of the chirped pulse was cycled (0°, 90°, 180°, 270°), which allowed sideband separation and the suppression of spurious harmonics.

Astronomical observations

We analysed a new unbiased, ultradeep molecular line survey conducted towards the Galactic Centre molecular cloud G+0.693 using the Yebes 40-m (Guadalajara, Spain) and the IRAM 30-m (Granada, Spain) radio telescopes. This broadband survey spanned a frequency range of ~91 GHz and had higher sensitivity compared with the data used in previous works (for example, ref. 12). The observations were carried out in position switching mode towards the equatorial coordinates of G+0.693 (right ascension α = 17 h 47 min 22 s and declination δ = −28° 21′ 27″) using an off position shifted by $\Delta\alpha$ = −885″ and $\Delta\delta$ = 290″.

Yebes 40-m radio telescope. New Yebes 40-m observing runs (Project 21A014; PI V. M. Rivilla) were performed between March 2021 and March 2022. We used the ultra-broadband Nanocosmos Q-band (7 mm) high electron mobility transistor (HEMT) receiver, which enables broadband observations across the whole Q-band (18.5 GHz between 31.07 GHz and 50.42 GHz) in two linear polarizations[56]. The 16 fast Fourier transform spectrometers provided a raw channel width of 38 kHz. We used two distinct spectral set-ups, centred at 41.4 GHz and 42.3 GHz, to identify possible spurious lines. The detailed procedure employed for the data reduction, combination and averaging of both the new Yebes 40-m and the IRAM 30-m data is presented in ref. 34. Subsequently, the spectra were imported into MADCUBA[43] and smoothed to a frequency resolution of 256 kHz (velocity resolutions of 1.5–2.5 km s^{-1} in the range observed). An extraordinary sensitivity has been reached, with r.m.s. noise levels ranging between 0.25 mK and 0.9 mK across the whole Q-band at this spectral resolution in units of the antenna temperature scale (T_A^*), as the molecular emission towards G+0.693 is extended over the beam[57]. The half-power beam-width of the telescope ranged between ~35″ and ~55″ (at 50 GHz and 31 GHz, respectively).

IRAM 30-m radio telescope. The new IRAM 30-m observations (Project 123-22; PI Jiménez-Serra) were carried out between 1 and 18 February 2023. We employed the multiband millimetre-wave eight mixer receiver and various frequency set-ups to cover three frequency windows, 83.2–115.41 GHz, 132.28–140.39 GHz and 142–173.81 GHz. Each frequency set-up was shifted in frequency to identify possible contamination of spurious lines coming from the image band. We achieved an initial spectral resolution of 195 kHz using a fast Fourier transform spectrometer (FTS200), even though we finally smoothed the spectra within MADCUBA to 615 kHz, which translates to velocity resolutions of 1.0–2.2 km s^{-1} in the observed frequency range. The half-power beam-width of the telescope varied between 14″ and 29″ across the frequency range covered. We note that for those frequency ranges that are not covered within these new data, we used the previous IRAM 30-m survey (further details are given elsewhere; for example, ref. 12). Overall, we obtained final noise levels between 0.5 mK and 2.5 mK at 3 mm and between 1.0 mK and 1.6 mK at 2 mm per channel.

LTE analysis of 2,5-CT with MADCUBA

Once the rotational spectroscopic data of 2,5-CT had been imported into the MADCUBA software package[43], we used the SLIM tool (version dated 15 June 2024) within MADCUBA to analyse the astronomical data under the assumption of LTE. We generated the LTE simulated spectra with SLIM and then conducted a nonlinear least-squares LTE fit of the brightest transitions of 2,5-CT that were either unblended or exhibited a slight blending (shown in Fig. 1 and listed in Extended Data Table 2) to the observed spectra using the AUTOFIT tool within SLIM[43]. The selection of these lines followed the criteria established in previous works[10,36] to identify unblended lines while considering potential contamination from a yet unidentified line. To evaluate the level of line blending, we analysed the region surrounding the 2,5-CT lines within a velocity range of ±FWHM/2, where FWHM represents the observed linewidth. The level of contamination was assessed by subtracting the LTE fit for 2,5-CT from the observed spectrum and calculating the residual area. The contributions to the residuals for all the selected lines are shown in Extended Data Table 2. A line was classified as unblended if the residual area contributed 25% or less to the total. Additionally, if a known molecule that lies within this range contributed less than 25% of the total integrated intensity, the line was considered to be slightly blended. The SLIM-AUTOFIT method enables us to derive the following physical parameters: molecular column density (N), excitation temperature (T_{ex}), radial velocity (υ_{LSR}) and FWHM. Only the latter parameter was fixed in the fit to a value of 20 km s^{-1} to achieve convergence, which is in agreement with the characteristic FWHM measured for the molecular transitions in G+0.693 (FWHM ≈ 15–20 km s^{-1}; see for example, ref. 39). We, thus, derived the following parameters: $N = (5.6 \pm 0.3) \times 10^{12}$ cm^{-2}, $T_{ex} = 14.3 \pm 3.4$ K and $\upsilon_{LSR} = 71.7 \pm 0.9$ km s^{-1}.

Rotational diagram analysis

As an alternative to the SLIM-AUTOFIT analysis, we can profit from applying the rotational diagram method[46] to derive the physical parameters of 2,5-CT. We used the reduced subset of clean and slightly blended transitions listed in Extended Data Table 2, excluding the transitions for which the contamination by an unidentified line accounted for >25% of the overall area, We obtained results that are in good agreement with both the column density and excitation temperature obtained using SLIM-AUTOFIT: $N = (5.6 \pm 1.4) \times 10^{12}$ cm^{-2} and $T_{ex} = 12.5 \pm 1.5$ K. The results of the rotational diagram method are shown in Extended Data Fig. 4.

Non-detection of 2,4-CT and thiophenol

We implemented in MADCUBA-SLIM the newly measured rotational data for 2,4-CT and searched for it in the survey towards G+0.693. 2,4-CT was not clearly detected, despite the emergence of several weak and unblended transitions within the noise. However, unlike 2,5-CT, it lacks clear enough spectroscopic features in the astronomical data for a conclusive detection. Therefore, we used the LTE parameters obtained for 2,5-CT to derive the upper limit for its molecular abundance. We searched for the brightest predicted spectral features of 2,4-CT that seem to be completely unblended with emission from other molecules previously identified in the astronomical data. Specifically, we used the $13_{0,13}$–$12_{0,12}$ transition (at ~33.677 GHz), which is one of the frequency regions of the survey with the highest sensitivity (r.m.s. ≈ 0.5 mK), which enabled us to place stringent constraints on the abundance of 2,4-CT towards G+0.693. We, thus, derived a 3σ upper limit for its column density (σ is the r.m.s. noise of the spectra) of $N \leq 3.2 \times 10^{12}$ cm^{-2}, which yields an upper limit for the molecular abundance with respect to molecular hydrogen of 2.7×10^{-11} and does not produce any overly bright features at other frequencies. Based on the derived upper limit, 2,4-CT is a factor of ~2 less abundant than 2,5-CT.

We also searched for thiophenol using available laboratory rotational data[58], without yielding a detection. Therefore, we derived the 3σ upper limit for its molecular abundance using the $15_{1,14}$–$14_{1,13}$ transition (at ~40.906 GHz), which is the brightest transition and a fully unblended transition predicted by the LTE model. We obtained $N \leq 8 \times 10^{13}$ cm^{-2} by adopting the physical parameters found for 2,5-CT. In terms of the molecular abundance with respect to H_2, the above value translates

into an upper limit of 6×10^{-10}. Thus, we found that thiophenol is ≤14 times more abundant than 2,5-CT, in line with the energy ordering of the three structural isomers (Extended Data Fig. 1).

Data availability

This paper makes use of data from projects 018-19, 123-22 and 076-23 (IRAM 30-m), and 21A014 (Yebes 40-m). The observed spectra and fits of the transitions of the different species presented in this work are available via Zenodo at https://doi.org/10.5281/zenodo.17598371 (ref. 59). The rotational lines of 2,5-CT and 2,4-CT are provided as Supplementary Data 1 and 2.

Code availability

The MADCUBA package, which was used to perform the LTE analysis performed in this work, is software publicly available at https://cab.inta-csic.es/madcuba/download.html. A description of the package is provided in ref. 43.

References

1. Oparin, A. I. & Morgulis, S. *The Origin of Life* (Macmillan, 1938).
2. Delsemme, A. H. Cometary origin of the biosphere. *Icarus* **146**, 313–325 (2000).
3. Osinski, G. R., Cockell, C. S., Pontefract, A. & Sapers, H. M. The role of meteorite impacts in the origin of life. *Astrobiology* **20**, 1121–1149 (2020).
4. Crovisier, J. et al. The composition of ices in comet C/1995 O1 (Hale-Bopp) from radio spectroscopy. *Astron. Astrophys.* **418**, 1141–1157 (2004).
5. Altwegg, K. et al. Prebiotic chemicals—amino acid and phosphorus—in the coma of comet 67P/Churyumov-Gerasimenko. *Sci. Adv.* **2**, e1600285 (2016).
6. Yabuta, H., Williams, L. B., Cody, G. D., Alexander, C. M. O. D. & Pizzarello, S. The insoluble carbonaceous material of CM chondrites: a possible source of discrete organic compounds under hydrothermal conditions. *Meteorit. Planet. Sci.* **42**, 37–48 (2007).
7. Oba, Y., Takano, Y., Dworkin, J. P. & Naraoka, H. Ryugu asteroid sample return provides a natural laboratory for primordial chemical evolution. *Nat. Commun.* **14**, 3107 (2023).
8. Connolly, H. C. Jr et al. An overview of the petrography and petrology of particles from aggregate sample from asteroid Bennu. *Meteorit. Planet. Sci.* **60**, 979–996 (2025).
9. Todd, Z. R. Sources of nitrogen-, sulfur-, and phosphorus-containing feedstocks for prebiotic chemistry in the planetary environment. *Life* **12**, 1268 (2022).
10. Sanz-Novo, M. et al. On the abiotic origin of dimethyl sulfide: discovery of dimethyl sulfide in the interstellar medium. *Astrophys. J. Lett.* **980**, L37 (2025).
11. Kolesniková, L. et al. Spectroscopic characterization and detection of ethyl mercaptan in Orion. *Astrophys. J. Lett.* **784**, L7 (2014).
12. Rodríguez-Almeida, L. F. et al. Thiols in the interstellar medium: first detection of HC(O)SH and confirmation of C_2H_5SH. *Astrophys. J. Lett.* **912**, L11 (2021).
13. Fuente, A. et al. Gas phase elemental abundances in molecular clouds (GEMS). VII. Sulfur elemental abundance. *Astron. Astrophys.* **670**, A114 (2023).
14. Orthous-Daunay, F.-R. et al. Speciation of sulfur in the insoluble organic matter from carbonaceous chondrites by XANES spectroscopy. *Earth Planet. Sci. Lett.* **300**, 321–328 (2010).
15. Mojarro, A. et al. Murchison meteorite analysis using tetramethylammonium hydroxide (TMAH) thermochemolysis under simulated sample analysis at Mars (SAM) pyrolysis-gas chromatography-mass spectrometry conditions. *J. Geophys. Res.: Planets* **128**, e2023JE007968 (2023).
16. Araki, M. List of observed interstellar molecules. https://molecules-in.space/ (2025).
17. McGuire, B. A. 2021 census of interstellar, circumstellar, extragalactic, protoplanetary disk, and exoplanetary molecules. *Astrophys. J. Suppl. Ser.* **259**, 30 (2022).
18. McGuire, B. A. et al. Detection of the aromatic molecule benzonitrile (c-C_6H_5CN) in the interstellar medium. *Science* **359**, 202–205 (2018).
19. McGuire, B. A. et al. Detection of two interstellar polycyclic aromatic hydrocarbons via spectral matched filtering. *Science* **371**, 1265–1269 (2021).
20. Wenzel, G. et al. Detection of interstellar 1-cyanopyrene: a four-ring polycyclic aromatic hydrocarbon. *Science* **386**, 810–813 (2024).
21. Wenzel, G. et al. Detections of interstellar aromatic nitriles 2-cyanopyrene and 4-cyanopyrene in TMC-1. *Nat. Astron.* **9**, 262–270 (2025).
22. Wenzel, G. et al. Discovery of the seven-ring polycyclic aromatic hydrocarbon cyanocoronene ($C_{24}H_{11}CN$) in GOTHAM observations of TMC-1. *Astrophys. J. Lett.* **984**, L36 (2025).
23. Loru, D., Cabezas, C., Cernicharo, J., Schnell, M. & Steber, A. L. Detection of ethynylbenzene in TMC-1 and the interstellar search for 1, 2-diethynylbenzene. *Astron. Astrophys.* **677**, A166 (2023).
24. Cernicharo, J. et al. Pure hydrocarbon cycles in TMC-1: discovery of ethynyl cyclopropenylidene, cyclopentadiene, and indene. *Astron. Astrophys.* **649**, L15 (2021).
25. Cernicharo, J. et al. Infrared Space Observatory's discovery of C_4H_2, C_6H_2, and benzene in CRL 618. *Astrophys. J.* **546**, L123 (2001).
26. Yang, X. J., Hua, L. & Li, A. Where have all the sulfur atoms gone? Polycyclic aromatic hydrocarbon as a possible sink for the missing sulfur in the interstellar medium. I. The C–S band strengths. *Astrophys. J.* **974**, 30 (2024).
27. Remijan, A. J. et al. The missing link of sulfur chemistry in TMC-1: the detection of c-C_3H_2S from the GOTHAM survey. *Astrophys. J.* **982**, 191 (2025).
28. McCarthy, M. C. et al. Exhaustive product analysis of three benzene discharges by microwave spectroscopy. *J. Phys. Chem. A* **124**, 5170–5181 (2020).
29. Cernicharo, J. et al. Discovery of two isomers of ethynyl cyclopentadiene in TMC-1: abundances of CCH and CN derivatives of hydrocarbon cycles. *Astron. Astrophys.* **655**, L1 (2021).
30. McCarthy, M. C. et al. Interstellar detection of the highly polar five-membered ring cyanocyclopentadiene. *Nat. Astron.* **5**, 176–180 (2021).
31. Lee, K. L. K. et al. Interstellar detection of 2-cyanocyclopentadiene, C_5H_5CN, a second five-membered ring toward TMC-1. *Astrophys. J. Lett.* **910**, L2 (2021).
32. Rivilla, V. M. et al. Precursors of the RNA world in space: detection of (*Z*)-1,2-ethenediol in the interstellar medium, a key intermediate in sugar formation. *Astrophys. J. Lett.* **929**, L11 (2022).
33. Jiménez-Serra, I. et al. Precursors of fatty alcohols in the ISM: discovery of n-propanol. *Astron. Astrophys.* **663**, A181 (2022).
34. Rivilla, V. M. et al. First glycine isomer detected in the interstellar medium: glycolamide ($NH_2C(O)CH_2OH$). *Astrophys. J. Lett.* **953**, L20 (2023).
35. San Andrés, D. et al. First detection in space of the high-energy isomer of cyanomethanimine: H_2CNCN. *Astrophys. J.* **967**, 39 (2024).
36. Rey-Montejo, M. et al. Discovery of MgS and NaS in the interstellar medium and tentative detection of CaO. *Astrophys. J.* **975**, 174 (2024).
37. Sanz-Novo, M. et al. Interstellar detection of O-protonated carbonyl sulfide, $HOCS^+$. *Astrophys. J.* **965**, 149 (2024).

38. Sanz-Novo, M. et al. Discovery of thionylimide, HNSO, in space: the first N-, S-, and O-bearing interstellar molecule. *Astrophys. J. Lett.* **965**, L26 (2024).
39. Zeng, S. et al. Complex organic molecules in the Galactic Centre: the N-bearing family. *Mon. Not. R. Astron. Soc.* **478**, 2962–2975 (2018).
40. Programs augmenting H.M. Pickett's SPFIT/SPCAT. *Institute of Physics, Polish Academy of Sciences* http://info.ifpan.edu.pl/%7Ekisiel/asym/asym.htm#piform (2022).
41. Yanai, T., Tew, D. P. & Handy, N. C. A new hybrid exchange–correlation functional using the Coulomb-attenuating method (cam-b3lyp). *Chem. Phys. Lett.* **393**, 51–57 (2004).
42. Woon, D. E. & Dunning, T. H. Jr. Gaussian basis sets for use in correlated molecular calculations. V. Core-valence basis sets for boron through neon. *J. Chem. Phys.* **103**, 4572–4585 (1995).
43. Martín, S. et al. Spectral Line Identification and Modelling (SLIM) in the Madrid Data Cube Analysis (MADCUBA) package. Interactive software for data cube analysis. *Astron. Astrophys.* **631**, A159 (2019).
44. Colzi, L. et al. Excitation and spatial study of a prestellar cluster towards G+0.693-0.027 in the Galactic Centre. *Astron. Astrophys.* **690**, A121 (2024).
45. Martín, S., Requena-Torres, M. A., Martín-Pintado, J. & Mauersberger, R. Tracing shocks and photodissociation in the Galactic Center region. *Astrophys. J.* **678**, 245–254 (2008).
46. Goldsmith, P. F. & Langer, W. D. Population diagram analysis of molecular line emission. *Astrophys. J.* **517**, 209–225 (1999).
47. Kocheril, G. S., Zagorec-Marks, C. & Lewandowski, H. J. Termination of bottom-up interstellar aromatic ring formation at $C_6H_5^+$. *Nat. Astron.* **9**, 685–691 (2025).
48. Zhou, L. et al. Cosmic-ray-mediated formation of benzene on the surface of Saturn's moon Titan. *Astrophys. J.* **718**, 1243–1251 (2010).
49. Cernicharo, J. et al. TMC-1, the starless core sulfur factory: discovery of NCS, HCCS, H_2CCS, H_2CCCS, and C_4S and detection of C_5S. *Astron. Astrophys.* **648**, L3 (2021).
50. Zeng, S. et al. Cloud-cloud collision as drivers of the chemical complexity in Galactic Centre molecular clouds. *Mon. Not. R. Astron. Soc.* **497**, 4896–4909 (2020).
51. Jose, J., Zamir, A. & Stein, T. Molecular dynamics reveals formation path of benzonitrile and other molecules in conditions relevant to the interstellar medium. *Proc. Natl Acad. Sci. USA* **118**, e2101371118 (2021).
52. Lee, K. L. K., McGuire, B. A. & McCarthy, M. C. Gas-phase synthetic pathways to benzene and benzonitrile: a combined microwave and thermochemical investigation. *Phys. Chem. Chem. Phys.* **21**, 2946–2956 (2019).
53. Gagonova, M. Y., Tyurin, D. A., Baranova, I. A. & Feldman, V. I. Radiation-induced transformations of an isolated $C_6H_6\cdots HCN$ complex: possible way to synthesis of interstellar benzonitrile. *J. Phys. Chem. A* **129**, 282–287 (2024).
54. Neese, F., Wennmohs, F., Becker, U. & Riplinger, C. The ORCA quantum chemistry program package. *J. Chem. Phys.* **152**, L224108 (2020).
55. Lattanzi, V. et al. $HSCO^+$ and $DSCO^+$: a multi-technique approach in the laboratory for the spectroscopy of interstellar ions. *Astron. Astrophys.* **620**, A184 (2018).
56. Tercero, F. et al. Yebes 40 m radio telescope and the broad band Nanocosmos receivers at 7 mm and 3 mm for line surveys. *Astron. Astrophys.* **645**, A37 (2021).
57. Zheng, S. et al. Mapping observations of peptide-like molecules around Sagittarius B2. *Astrophys. J.* **961**, 58 (2024).
58. Larsen, N. W. & Schulz, L. Internal rotation and structure of thiophenol and 4-fluorothiophenol studied by microwave spectroscopy and quantum chemistry. *J. Mol. Struct.* **920**, 30–39 (2009).
59. Araki, M. et al. A detection of sulfur-bearing cyclic hydrocarbons in space. *Zenodo* https://doi.org/10.5281/zenodo.17598371 (2026).
60. Pickett, H. M. The fitting and prediction of vibration-rotation spectra with spin interactions. *J. Mol. Spectrosc.* **148**, 371–377 (1991).

Acknowledgements

M.A., C.P.E., V.L. and P.C. acknowledge the the financial support of the Max Planck Society. This paper makes use of data from Projects 018-19, 123-22 and 076-23 (IRAM 30-m) and 21A014 (Yebes 40-m). The 40 m radio telescope at Yebes Observatory is operated by the Spanish Geographic Institute (IGN, Ministerio de Transportes, Movilidad y Agenda Urbana). IRAM is supported by INSU/CNRS (France), MPG (Germany) and IGN (Spain). M.S.-N. acknowledges a Juan de la Cierva Postdoctoral Fellow project JDC2022-048934-I, funded by the Spanish Ministry of Science, Innovation and Universities/State Agency of Research MICIU/AEI/10.13039/501100011033 and by the European Union NextGenerationEU/PRTR. V.M.R. acknowledges support from the grant RYC2020-029387-I funded by MICIU/AEI/10.13039/501100011033 and by ESF, Investing in Your Future, from the Consejo Superior de Investigaciones Científicas (CSIC) and the Centro de Astrobiología through the project 20225AT015 (Proyectos intramurales especiales del CSIC), and from the grant CNS2023-144464 funded by MICIU/AEI/10.13039/501100011033 and by European Union NextGenerationEU/PRTR. D.S.A. acknowledges support from Grant No. CNS2023-144464. I.J.-S., V.M.R., M.S.-N., L.C, A.M., A.L.-G., A.M.-H. and D.S.A. acknowledge funding from Grant No. PID2022-136814NB-I00 from MICIU/AEI/10.13039/501100011033 and from ERDF, UE A way of making Europe. I.J.-S. acknowledges funding from the ERC grant OPENS (Project No. 101125858) funded by the European Union. The views and opinions expressed are, however, those of the authors only and do not necessarily reflect those of the European Union or the European Research Council Executive Agency. Neither the European Union nor the granting authority can be held responsible for them. M.S.-N., I.J.-S., L.C. and S.Z. acknowledge funding from CSIC through project i-LINK23017 SENTINEL. D.S.A. expresses his gratitude for the funds from the Comunidad de Madrid through Grant PIPF-2022/TEC-25475 and the financial support of CSIC and the Centro de Astrobiología through project 20225AT015 (Proyectos intramurales especiales del CSIC). S.Z. acknowledges the support of the RIKEN Special Postdoctoral Researchers Program. J.G.d.l.C. acknowledges support from Grant No. PID2022-136814NB-I00 287 from MICIU/AEI/10.13039/501100011033 and from ERDF, UE A way of making Europe. J.G.d.l.C. also acknowledges support from European Funds for Regional Development and the Autonomous Government of Extremadura (Grant No. GR24020).

Author contributions

M.A. and C.P.E. performed the laboratory experiments and collected the data. M.A. and V.L. carried out the theoretical calculations. C.P.E. analysed the laboratory data. V.L. and P.C. coordinated the project. M.S.-N., V.M.R., I.J.-S., L.C., S.Z., A.M., A.L.-G., A.M.-H., D.S.A., S.M., M.A.R.-T. and J.G.d.l.C. contributed to the collection and reduction of the astronomical data. V.M.R. and I.J.-S. led the observational survey. M.S.-N. analysed the astronomical observations. M.A. and M.S.-N. wrote the paper with the help of V.L. All authors provided feedback and commented on the paper.

Funding

Open access funding provided by Max Planck Society.

Competing interests

The authors declare no competing interests.

Additional information

Extended data is available for this paper at https://doi.org/10.1038/s41550-025-02749-7.

Supplementary information The online version contains supplementary material available at https://doi.org/10.1038/s41550-025-02749-7.

Correspondence and requests for materials should be addressed to Mitsunori Araki or Valerio Lattanzi.

Peer review information *Nature Astronomy* thanks the anonymous reviewers for their contribution to the peer review of this work.

https://doi.org/10.1038/s41550-025-02749-7

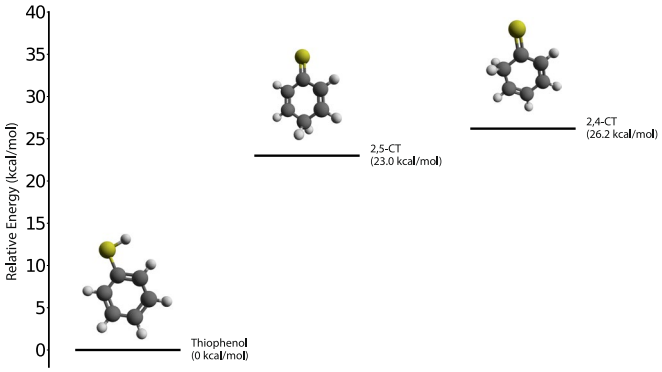

Extended Data Fig. 1 | Energy levels of 2,5-CT and 2,4-CT relative to thiophenol. The geometries and energies were derived at the CAM-B3LYP/cc-pCV5Z level of theory.

https://doi.org/10.1038/s41550-025-02749-7

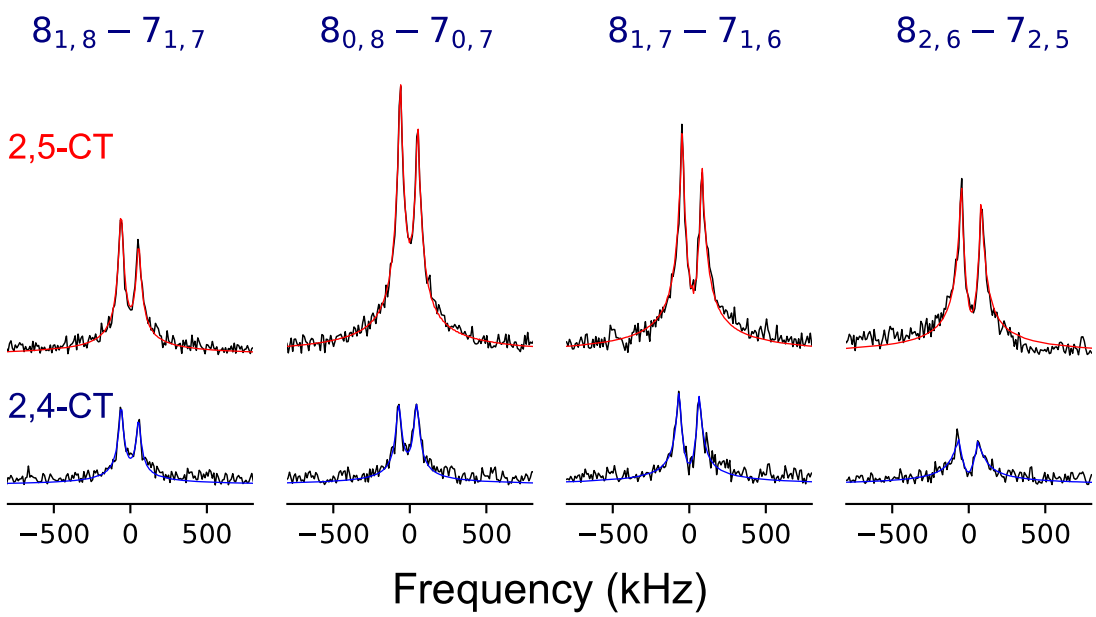

Extended Data Fig. 2 | Sections of the experimental spectrum (black), showing four transitions for each of the two molecules 2,4-CT and 2,5-CT with corresponding quantum numbers $J'_{Ka',Kc'} - J''_{Ka'',Kc''}$ given in the top trace. The adapted line profile fit is shown in color. The frequency axis is centered on the predicted transition frequency in each case. The Doppler effect causes a double peak profile with a splitting of about 100 kHz due to the optical alignment.

https://doi.org/10.1038/s41550-025-02749-7

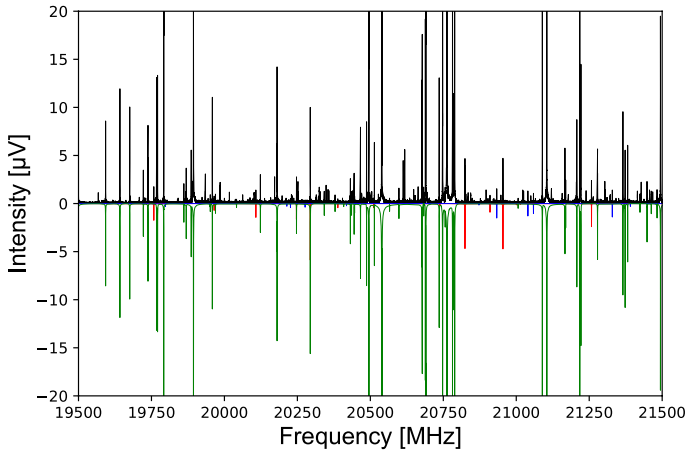

Extended Data Fig. 3 | Section of the experimental spectrum (black, upward), showing the frequency range between 19500–21500 MHz. The adapted line profile fit for selected species is shown in color (green: Thiophenol, black: ^{34}S-Thiophenol, red: 2,5-CT, blue: 2,4-CT) with inverted intensities.

https://doi.org/10.1038/s41550-025-02749-7

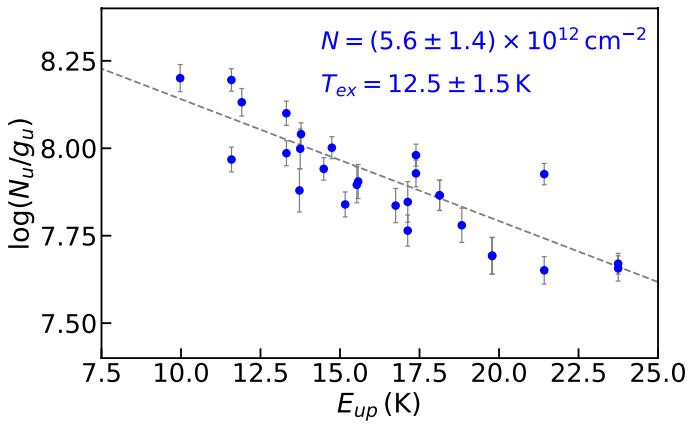

Extended Data Fig. 4 | Rotational diagram for the selected transitions of 2,5-CT (depicted in Fig. 1) observed toward G+0.693. Data points (blue dots) are presented as mean values ± standard errors of the means (1σ errors). The best linear fit to the data points is shown using a gray dashed line. The values for the molecular column density, N, and the excitation temperature, T_{ex}, obtained from the fit are shown in blue.

https://doi.org/10.1038/s41550-025-02749-7

Extended Data Table 1 | Energies and dipole moments for the thiophenol system

Species	Energy [a.u.]	Rel. En. [kcal/mol]	μ_a [D]	μ_b [D]
Thiophenol	-630.4423497	0.0	0.83	0.75
2,5-CT	-630.4056913	23.0	4.73	
2,4-CT	-630.4005289	26.2	3.87	0.44

All the calculations were performed with ORCA using the CAM-B3LYP method and the cc-pCV5Z basis set.

https://doi.org/10.1038/s41550-025-02749-7

Extended Data Table 2 | Spectroscopic information of the brightest and cleanest detected transitions of 2,5-CT toward G+0.693 − 0.027, which are shown in Fig. 1 and were used to derive the physical parameters of the molecule

Frequency (GHz)	Transition[a]	log I (300 K) (nm^2 MHz)	E_{up} (K)	rms (mK)	$\int T_A^* dv$ (mK km s^{-1})	Residual area [b] (%)	S/N [c]	Blending
31.0816996 (13)	$12_{0,12}$–$11_{0,11}$	–5.2700	9.9	0.6	32.2	24.2	10.4	Unblended
31.5304333 (33)	$11_{7,5}$–$10_{7,4}$	–5.4181	18.0	0.6	27.0	24.4	8.7	Unblended*
31.5304364 (33)	$11_{7,4}$–$10_{7,3}$	–5.4181	18.0	0.6				Unblended*
33.5137909 (15)	$13_{1,13}$–$12_{1,12}$	–5.0626	11.5	0.5	26.3	5.7	10.7	Unblended
33.5538160 (15)	$13_{0,13}$–$12_{0,12}$	–5.1707	11.5	0.5	40.3	7.0	16.4	Slightly blended: CH_3COCH_3
34.4218320 (35)	$12_{7,6}$–$11_{7,5}$	–5.2616	19.6	0.5	20.4	8.5	7.7	Unblended*
34.4218433 (35)	$12_{7,5}$–$11_{7,4}$	–5.2616	19.6	0.5				Unblended*
34.4802711 (23)	$12_{6,7}$–$11_{6,6}$	–5.3101	17.3	0.5	24.9	19.3	9.3	Unblended*
34.4808071 (23)	$12_{6,6}$–$11_{6,5}$	–5.3101	17.3	0.5				Unblended*
34.6646714 (10)	$12_{4,9}$–$11_{4,8}$	–5.2266	13.6	0.5	20.1	9.5	7.5	Unblended
34.9060892 (13)	$12_{4,8}$–$11_{4,7}$	–5.2206	13.7	0.5	20.2	7.3	7.6	Unblended
36.0055197 (19)	$14_{1,14}$–$13_{1,13}$	–4.9702	13.2	0.4	27.4	3.0	12.1	Unblended
36.0303689 (19)	$14_{0,14}$–$13_{0,13}$	–5.0787	13.2	0.4	61.6	11.0	27.2	Blended: $OC^{33}S$
36.0334115 (18)	$12_{2,10}$–$11_{2,9}$	–5.1522	11.8	0.4	30.3	6.8	13.3	Unblended
37.5869628 (14)	$13_{4,10}$–$12_{4,9}$	–5.1162	15.4	0.4	28.8	32.9	12.7	Blended: U-line
37.9936987 (20)	$13_{4,9}$–$12_{4,8}$	–5.1068	15.5	0.4	24.5	22.7	10.7	Unblended
38.4947436 (26)	$15_{1,15}$–$14_{1,14}$	–4.8845	15.1	0.3	31.4	15.1	26.5	Slightly blended: U-line
38.7357999 (21)	$14_{1,13}$–$13_{1,12}$	–4.9158	14.6	0.3	47.6	31.4	15.0	Blended: U-line
38.8332164 (22)	$13_{2,11}$–$12_{2,10}$	–5.0545	13.7	0.3	28.0	13.4	19.3	Unblended
39.0805294 (27)	$13_{3,10}$–$12_{3,9}$	–4.9508	14.4	0.3	50.5	15.6	7.9	Slightly blended: aGg'-$(CH_2OH)_2$
40.8344834 (28)	$15_{2,14}$–$14_{2,13}$	–4.9522	16.6	0.5	22.2	10.4	8.4	Unblended
40.9823609 (35)	$16_{1,16}$–$15_{1,15}$	–4.8046	17.0	0.5	39.3	7.1	14.9	Unblended
40.9915911 (35)	$16_{0,16}$–$15_{0,15}$	–4.9135	17.0	0.4	24.0	11.2	10.1	Unblended
43.3598980 (36)	$16_{2,15}$–$15_{2,14}$	–4.8742	18.7	0.4	36.6	9.5	15.3	Slightly blended: N-CH_3NHCHO
44.3536663 (46)	$15_{4,11}$–$14_{4,10}$	–4.9045	19.5	0.6	25.5	26.6	7.8	Slightly blended: U-line
45.9549697 (61)	$18_{1,18}$–$17_{1,17}$	–4.6597	21.3	0.9	56.7	3.9	11.1	Blended: $HOCH_2CN$
45.9582741 (61)	$18_{0,18}$–$17_{0,17}$	–4.7687	21.3	0.9	33.0	21.2	6.5	Unblended*
48.4405979 (78)	$19_{1,19}$–$18_{1,18}$	–4.5935	23.6	1.1	33.2	12.6	5.4	Unblended*
48.4425540 (78)	$19_{0,19}$–$18_{0,18}$	–4.7026	23.6	1.1				Unblended*

Note: [a] The rotational energy levels are labeled using the conventional notation for asymmetric tops: J_{K_a,K_c}, where J denotes the angular momentum quantum number, and the K_a and K_c labels are projections of J along the a and c principal axes. [b] We give the contribution of the (unknown) contamination to the overall area after subtracting the LTE fit of 2,5-CT from the observed spectrum, including also the contribution from all the molecules previously detected in the molecular line survey of G+0.693. [c] The S/N ratio is computed from the integrated signal ($\int T_A^* dv$) and noise level, σ = rms $\times\sqrt{\delta v \times \mathrm{FWHM}}$, where δv is the velocity resolution of the spectra and the FWHM is fitted from the data. Transitions with the * symbol are (auto)blended with another transition of 2,5-CT. Numbers in parentheses represent the predicted uncertainty associated to the last digits.

https://doi.org/10.1038/s41550-025-02749-7

Extended Data Table 3 | Total nuclear-spin rotational partition functions of 2,5- and 2,4-cyclohexadien-1-thione

Temperature (K)	2,5-CT	2,4-CT
300.0	8 630 336.0532	17 280 951.3727
225.0	5 604 765.7502	11 222 535.6993
150.0	3 050 479.2413	6 107 946.6382
75.0	1 078 472.3004	2 159 384.3021
37.5	381 367.1993	763 592.2474
18.75	134 899.6435	270 102.2843
9.375	47 743.8953	95 595.2424

Note. Statistical weights for even and odd states are 28:36 and 64:64 for 2,5-CT and 2,4-CT, respectively. Partition functions take only vibrational ground state and rotational states up to J_{max}=300 into account.